machines

MDPI

Article

A Method for Solving the Additional Stiffness Introduced by Flexible Joints in Stewart Platform Based on FEM Modal Analysis

Tianqing Zhang [1,2], Xiaoxue Gong [3], Lei Zhang [1,2,3,*], Yuzhe Wang [1,2], Yahui Liu [3] and Lin Li [4,5]

1 Changchun Institute of Optics, Fine Mechanics and Physics, Changchun 130000, China
2 University of Chinese Academy of Sciences, Beijing 100049, China
3 Chang Guang Satellite Technology Co., Ltd., Changchun 130000, China
4 Space Optoelectronic Measurement and Perception Lab., Beijing Institute of Control Engineering, Beijing 100190, China
5 China Academy of Space Technology, Beijing 100094, China
* Correspondence: zhanglei@charmingglobe.com

Abstract: The usage of flexible joints has greatly facilitated the widespread application of the Stewart construction mechanism in many advanced fields. This research focuses on the problem that the flexible joints in the Stewart mechanism cause additional stiffness effects on the whole system. A method for solving the additional stiffness of flexible joints combining the finite element method (FEM) is proposed, which avoids the complex theoretical derivation process and allows the advantages of high versatility and accuracy. Three aspects make up the main content. Firstly, based on dynamics theory, the theoretical analysis and demonstration of the method are conducted according to the symmetry characteristics of the Stewart platform. Next, the additional stiffness of a designed Stewart platform with flexible joints was solved following the method proposed, and the obtained results were verified through FEM simulation under the given conditions, which give a maximum natural frequency deviation against the theory of 2.26%. Thirdly, dynamics tests associated with the Stewart platform were conducted, and the deviation between the Stewart Platform's natural frequencies separately obtained from the tests and the theory does not exceed 5%, which demonstrates the effectiveness and accuracy of the method in engineering applications. This study aims to provide technical support for the development of Stewart mechanisms with flexible joints.

Keywords: Stewart platform; flexible joint; modal analysis; stiffness calculation; FEM analysis

Citation: Zhang, T.; Gong, X.; Zhang, L.; Wang, Y.; Liu, Y.; Li, L. A Method for Solving the Additional Stiffness Introduced by Flexible Joints in Stewart Platform Based on FEM Modal Analysis. *Machines* **2023**, *11*, 457. https://doi.org/10.3390/machines11040457

Academic Editor: Zhuming Bi

Received: 27 February 2023
Revised: 31 March 2023
Accepted: 31 March 2023
Published: 4 April 2023

1. Introduction

Since the Gough-Stewart configuration parallel platform was proposed in the 1960s [1], there has been considerable research work by scholars on the theoretical modeling, motion simulation and mechanical testing of this interesting mechanism [2]. Owing to the excellent multidimensional motion characteristic of the Stewart configuration mechanism, the application of the mechanism has spread across many fields, such as biomedical devices, aerospace engineering and industrial manufacturing [3–5]. In the typical Stewart mechanism, the six legs are linked to the platform mainly by rigid joints, including ball joints and universal joints. Nevertheless, the relative movements of rigid parts occur during the working of rigid joints, which invariably cause nonlinear behavior of the system, such as clearances, friction and backlash [6]. This results in lower accuracy, lower smoothness and higher uncertainty of dynamic characteristics in the system, which greatly limits the application of the Stewart mechanism in situations with high requirements for precision or stability of motion.

To address this shortcoming, researchers have gradually shifted their research direction towards flexible joints to substitute the function of rigid joints installed on the

Stewart mechanism [7–14]. As a result, the working accuracy and dynamic characteristics of the Stewart mechanism have been substantially improved. Compared with the rigid joint, the flexible joint adopts an integrated design, which not only effectively avoids the inherent nonlinear behavior caused by structural clearances but also has the advantages of compactness and no lubrication [15]. Nowadays, research and applications around the Stewart mechanism installed with flexible joints have covered many important areas in engineering, such as multidimensional motion control [16–18], multidimensional disturbance suppression [19–21] and precision measurement systems [22–24]. However, with the usage of Flexible joints in the Stewart platform, a new difficulty had to be presented to the designers. It is well known that the flexible joint achieves relative motion between the connected parts through its own elastic deformation, and rebound forces are generated during the process, which leads to the introduction of the corresponding additional stiffness in the whole Stewart mechanism system. Consequently, the complexity of the dynamics theoretical analysis for the Stewart mechanism system is greatly increased.

Compared to the parallel legs in the Stewart platform, it is quite challenging to derive the additional stiffness matrix of the flexible joints. Therefore, when confronting the condition that the additional stiffness of Flexible joints has little effect, many researchers preferred to neglect the bending stiffness effect of Flexible joints during the theoretical study on Stewart configuration mechanisms [9,10,25–27]. Despite so, in certain applications with higher stiffness sensitivity as well as demanding operational accuracy requirements [28,29], researchers need to emphasize the influence of the stiffness brought by flexible joints in the Stewart mechanism to ensure the mechanical accuracy of the whole system.

There are currently many theoretical studies on Stewart mechanisms with flexible joints that consider the effect of flexible joint stiffness. Wang [30] represents the elastic bending and torsional deformation of the flexible joints by vector operations and establishes a standard dynamics formulation of the equivalent torque based on the principle of virtual work and the Lagrange method. Jiao [11], based on the Kane equation, derived the complete dynamics equations of the Stewart active vibration isolation platform with flexible joints by combining the principle of virtual work. To research the performance of the 6-UPUR type Stewart configuration 6-axis force sensor, based on the screw theory, Zhao [12] established a complete mathematical model of force transfer characteristics according to the relationship between stiffness and deformation compatibility conditions, which considers the stiffness of the flexible joints. To compensate for the added stiffness of the flexible joints in the control algorithm, Yang [13] first obtained a linearized explicit dynamics model of the flexible joint stiffness in the Stewart platform based on the pseudo-rigid-body model and the principle of virtual power. Yao [31] respectively constructed the overall stiffness matrix and the analytical mapping relationship of the 6-DOF force sensors based on the superposition principle under small deformations, which is certainly inspiring for the analysis of the stiffness of the flexure Stewart platform. As we can see from the above literature, it is a complicated and trying process to derive and analyze the stiffness participation of the flexible joints in a parallel mechanism through the dynamic theory approach. Additionally, due to the differences in application scenarios and designers' mindsets, there can be a variety of position distribution and structural forms of flexible joints, which results in various types of Stewart mechanisms with different motion characteristics. Therefore, the theoretical model built for a particular structure type Stewart platform inevitably has limitations, which greatly reduce its availability.

In addition to the theoretical approach, it is worth mentioning that finite element method (FEM) simulation also provides a direct and effective approach for the analysis of rigid-flexible coupling systems. Furqan [32] adopted the FEM simulation to solve the natural frequencies of the Stewart platform with flexible joints and obtained results comparable to the theory. DU [33] analyzed the stiffness and dynamic characteristics of the Stewart configuration precision pointing mechanism by means of FEM simulation. Ranganath [34] and Mohammed [35] respectively conducted the force sensitivity analysis of the Stewart configuration six-dimensional force sensors with FEM simulation. Nevertheless, the single FEM simulation can only serve for the resultant analysis, which lacks the ability to solve the dynamic parameters of the system, so it cannot be used directly to obtain the numerical results regarding the stiffness effects of the flexible joints in the Stewart platform system.

This study mainly focuses on the effects of additional stiffness generated by flexible joints in Stewart platforms. Based on the dynamics modal characteristics of the Stewart platform system, a method for solving the additional stiffness of flexible joints is proposed depending on the FEM simulation. Based on theoretical research, the method is systematically analyzed and demonstrated together with simulation analysis and dynamics tests, which completely as well as sufficiently illustrate the correctness and effectiveness of the method for practical engineering applications. Compared with traditional dynamics methods such as the Newton-Euler method and Lagrange principle, the method proposed avoids the introduction of constraint forces and redundant derivative calculations. While avoiding complex kinematic analysis and formula derivation, it also reduces the involvement of calculated parameters, thus reducing the introduction of measuring deviations from the actual values of the system, which ensures high accuracy of the solution results in engineering. Moreover, the method holds a high degree of generality in practical applications. Theoretically, under the basic premise of stiffness symmetry, the additional stiffness caused by flexible joints with different position distributions or various structural forms in the Stewart mechanism can be solved by the method, which makes it fairly versatile for applications. The state of the art of this paper is creating a method with high generality and accuracy for solving the additional stiffness of flexible joints in the Stewart platform from a new perspective of combining theoretical analysis with FEM simulation methods, which has a high operational feasibility in practical engineering. Related parameter design methods are original and haven't been proposed before. The paper provides certain technical references for the design and stiffness analysis of the Stewart configuration mechanism with flexible joints, further contributing to the Stewart configuration mechanism's research and development in various engineering fields.

The paper contains five sections. Section 2 elaborates on the method for solving the additional stiffness of flexible joints theoretically; Section 3 solves and verifies the additional stiffness of Flexible joints in the Stewart platform through FEM modal analysis; Section 4 presents the experimental work regarding the Stewart platform; Section 5 concludes the overall work of this paper.

2. Theoretical Analysis on Solving Additional Stiffness Introduced by Flexible Joints

2.1. Definitions of Coordinate Systems and Description of Key Parameters

The main structure of the Stewart platform is primarily composed of the upper platform, lower platform and parallel legs. The schematic diagram of the platform structure is shown in Figure 1a; the joint points where the upper and lower platforms are connected to the legs are P_i and B_i (i = 1~6) respectively, and they are separately distributed on the joint point circles of the upper and lower platforms. The centers of the upper and lower joint circles are respectively taken as the origins to establish the coordinate systems O_P-XYZ and O_B-XYZ, which are respectively fixed to the upper and lower platforms. The axes of both coordinate systems are oriented in the same direction, with the X- and Y-axes pointing horizontally and the Z-axis pointing vertically. Five main parameters are needed to determine the primary structure of the platform: the radius of the upper joint point circle R_P, the radius of the lower joint point circle R_B, the distribution angle of the upper joint point α, the distribution angle of the lower joint point β and the height difference between the upper and lower joint point circles H.

In the common Stewart platform of SPS (Spherical-prismatic-spherical) and UPS (Universal-prismatic-spherical) types, the connection between the legs and the platforms is usually adopted by ball hinges or universal hinges, neither of which creates an elastic force at the joint region, and the overall stiffness of the platform system can be treated as generated only by the axial stretching force of the legs. When flexible joints are adopted, the corresponding bending stiffness effects will be produced in the platform system. The schematic diagram of leg links with flexible joints is shown in Figure 1b. The stretching stiffness coefficient of each leg is: $k_{si} = k_s \ (i = 1 \sim 6)$, and the bending stiffness of each flexible joint is: $k_{Rj} = k_R \ (j = 1 \sim 12)$. This paper focuses on the system stiffness based on the modal analysis method, and the tiny damping coefficient of the flexible joints hardly has effects on the dynamical performance of the whole system, so the effect of system damping can be ignored during the process of theoretical analysis.

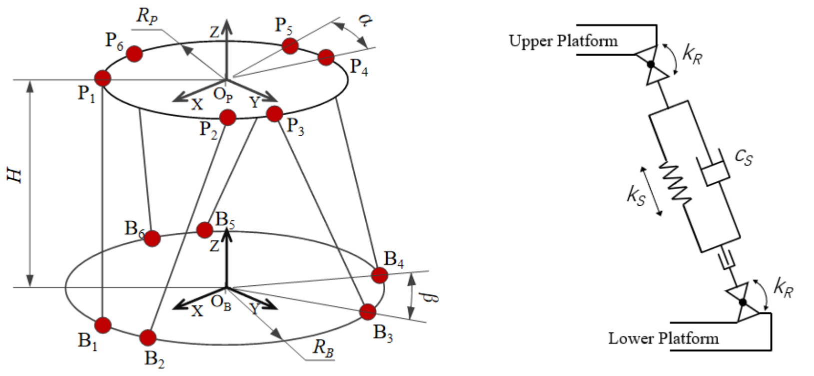

Figure 1. Structure diagram of Stewart platform: (**a**) Schematic diagram of platform structure; (**b**) Schematic diagram of platform leg link with Flexible joint.

2.2. Theoretical Analysis of Stewart Platform

First of all, we assume that the generalized coordinate vector of the upper platform is $X = [x_1\ x_2\ x_3\ x_4\ x_5\ x_6]$, where $[x_1\ x_2\ x_3]$ indicates the coordinates of the three translational directions of the upper platform, and $[x_4\ x_5\ x_6]$ represents the coordinates of the three rotation directions. The dynamics equation of the platform can be expressed as: $\boldsymbol{M\ddot{X}} + \boldsymbol{C\dot{X}} + \boldsymbol{KX} = 0$. In the present study, only the modal characteristics of the system are considered, so the damping term $\boldsymbol{C}$ in the formula is omitted here, and the equation can be written as:

$$\boldsymbol{M\ddot{X}} + \boldsymbol{KX} = 0 \tag{1}$$

where $\boldsymbol{M}$ is the generalized mass matrix of the system, and $\boldsymbol{K}$ is the generalized stiffness matrix of the system.

2.2.1. Analysis of Generalized Mass Matrix Characteristics

Here we first analyze the generalized quality matrix of system $\boldsymbol{M}$. In the case of considering only the upper platform and its load mass, the generalized mass matrix of the system is:

$$\boldsymbol{M} = \begin{bmatrix} m \cdot \boldsymbol{E_3} & m \cdot {}^{B}_{P}\boldsymbol{R} \cdot {}^{P}\widetilde{\boldsymbol{P}}_C{}^{T} \cdot {}^{P}_{B}\boldsymbol{R}^T \\ m \cdot {}^{B}_{P}\boldsymbol{R} \cdot {}^{P}\widetilde{\boldsymbol{P}}_C{}^{T} \cdot {}^{P}_{B}\boldsymbol{R}^T & {}^{B}_{P}\boldsymbol{R} \cdot {}^{P}\boldsymbol{I} \cdot {}^{P}_{B}\boldsymbol{R}^T \end{bmatrix} \tag{2}$$

where m denotes the quality of the upper platform, $\boldsymbol{E_3}$ is the matrix for the three-order unit, ${}^{B}_{P}\boldsymbol{R}$ is the rotation transformation matrix between the coordinate system O_P-XYZ and O_B-XYZ, ${}^{P}\widetilde{\boldsymbol{P}}_C$ denotes the skew-symmetric matrix of the coordinates of the integrated center of mass of the upper platform and its load in the dynamics coordinate system, and ${}^{P}\boldsymbol{I}$ denotes the inertia tensor of the upper platform and the load in the moving coordinate system O_P-XYZ.

By further analyzing Equation (2), we can see that when the mass characteristics of the upper platform and its load of the Stewart platform system satisfy certain symmetry conditions, the generalized mass matrix $\boldsymbol{M}$ of the system has the corresponding parametric characteristics. Moreover, when the load masses are symmetric about the X- and Y-axes, the generalized mass matrix $\boldsymbol{M}$ has the following form:

$$\boldsymbol{M} = \begin{bmatrix} M_{11} & 0 & 0 & 0 & M_{15} & 0 \\ 0 & M_{22} & 0 & M_{24} & 0 & 0 \\ 0 & 0 & M_{33} & 0 & 0 & 0 \\ 0 & M_{42} & 0 & M_{44} & 0 & 0 \\ M_{51} & 0 & 0 & 0 & M_{55} & 0 \\ 0 & 0 & 0 & 0 & 0 & M_{66} \end{bmatrix} \tag{3}$$

Here, the elements of the matrix $\boldsymbol{M}$ meet the following parameter characteristics: $M_{11} = M_{22} = M_{33} = m$; $M_{15} = M_{51}$, $-M_{24} = -M_{42}$.

2.2.2. Analysis of Generalized Stiffness Matrix Characteristics

The same analytical procedure is conducted for the generalized stiffness matrix $\boldsymbol{K}$. When the Stewart platform is installed with flexible joints, the overall stiffness of the system comes from two factors: the stretching stiffness of the outrigger leg and the bending stiffness of the flexible joint. In the Stewart platform, the outrigger legs and the flexible joints can be considered as two parallel sets of springs in the system so that their respective corresponding generalized stiffness in the system can be superimposed, and the generalized stiffness of the system can be obtained as follows:

$$\boldsymbol{K} = \boldsymbol{K_S} + \boldsymbol{K_R} \tag{4}$$

where $\boldsymbol{K_S}$ means the generalized stiffness introduced by the leg stiffness and $\boldsymbol{K_R}$ means the additional stiffness introduced by the flexible joint stiffness.

Next, a simple derivation of the stiffness matrix $\boldsymbol{K_S}$ is presented. The Jacobi matrix from a generalized displacement of the upper platform to the displacement of the supporting leg can be easily obtained:

$$\boldsymbol{J} = \begin{bmatrix} \boldsymbol{l}_{n1}^T & \left({}_P^B\boldsymbol{R}\cdot\boldsymbol{P}_1 \times \boldsymbol{l}_{n1}\right)^T \\ \boldsymbol{l}_{n2}^T & \left({}_P^B\boldsymbol{R}\cdot\boldsymbol{P}_2 \times \boldsymbol{l}_{n2}\right)^T \\ \boldsymbol{l}_{n3}^T & \left({}_P^B\boldsymbol{R}\cdot\boldsymbol{P}_3 \times \boldsymbol{l}_{n3}\right)^T \\ \boldsymbol{l}_{n4}^T & \left({}_P^B\boldsymbol{R}\cdot\boldsymbol{P}_4 \times \boldsymbol{l}_{n4}\right)^T \\ \boldsymbol{l}_{n5}^T & \left({}_P^B\boldsymbol{R}\cdot\boldsymbol{P}_5 \times \boldsymbol{l}_{n5}\right)^T \\ \boldsymbol{l}_{n6}^T & \left({}_P^B\boldsymbol{R}\cdot\boldsymbol{P}_6 \times \boldsymbol{l}_{n6}\right)^T \end{bmatrix} \tag{5}$$

where, $\boldsymbol{l_{ni}}$ $(i = 1 \sim 6)$ denotes the unit direction vector of each leg in the static coordinate system O_B-XYZ, and $\boldsymbol{P_i}$ is the position vector of the joint points of the upper platform in the dynamics coordinate system O_P-XYZ. The generalized stiffness matrix of the system caused by the leg stiffness is: $\boldsymbol{K_S} = \boldsymbol{J^T K_{SDiag} J}$, where $\boldsymbol{K_{SDiag}} = Diag(k_{s1}\ k_{s2}\ k_{s3}\ k_{s4}\ \ k_{s5}\ k_{s6})$. Substituting Equation (5) into the equation above, $\boldsymbol{K_S}$ can be obtained in the following form:

$$\boldsymbol{K_S} = \boldsymbol{J^T K_{SDiag} J} = \begin{bmatrix} K_{S11} & 0 & 0 & 0 & K_{S15} & 0 \\ 0 & K_{S22} & 0 & K_{S24} & 0 & 0 \\ 0 & 0 & K_{S33} & 0 & 0 & 0 \\ 0 & K_{S42} & 0 & K_{S44} & 0 & 0 \\ K_{S51} & 0 & 0 & 0 & K_{S55} & 0 \\ 0 & 0 & 0 & 0 & 0 & K_{S66} \end{bmatrix} \tag{6}$$

Through further derivation of the elements in Equation (6) based on the matrices J and K_{SDiag}, it can be proved that the stiffness matrix $\boldsymbol{K_S}$ satisfies the following parameter characteristics: $K_{S11} = K_{S22}$; $K_{S44} = K_{S55}$; $K_{S15} = K_{S51} = -K_{S24} = -K_{S42}$. In this case, the number of parameters in the stiffness matrix $\boldsymbol{K_S}$ can be reduced from 10 to 5. These parameter characteristics are mainly resulting from symmetry about the Z-axis and dynamics coupling characteristics of the Stewart platform, which has been approached in some studies [6,35], and it will not go into detail here.

With the similarity to the generalized mass matrix $\boldsymbol{M}$, the Stewart platform with flexible joints also has the same overall symmetry characteristics, so it can be inferred that the overall generalized stiffness matrix $\boldsymbol{K}$ has the same form as $\boldsymbol{K_S}$, which can be finally confirmed in the subsequent simulations and tests. Finally, the overall generalized stiffness matrix $\boldsymbol{K}$ of the system can be obtained in the following form:

$$\boldsymbol{K} = \begin{bmatrix} K_{11} & 0 & 0 & 0 & K_{15} & 0 \\ 0 & K_{22} & 0 & K_{24} & 0 & 0 \\ 0 & 0 & K_{33} & 0 & 0 & 0 \\ 0 & K_{42} & 0 & K_{44} & 0 & 0 \\ K_{51} & 0 & 0 & 0 & K_{55} & 0 \\ 0 & 0 & 0 & 0 & 0 & K_{66} \end{bmatrix} \tag{7}$$

Similarly, the elements in the generalized stiffness matrix $\boldsymbol{K}$ of the system are satisfied: $K_{11} = K_{22}$; $K_{44} = K_{55}$; $K_{15} = K_{51} = -K_{24} = -K_{42}$.

2.3. The Solution of Additional Stiffness of Flexible Joints

Next, the theoretical analysis of the Stewart platform continues based on the specific load quality conditions mentioned in Section 2.2.1. Under the conditions that the parameter properties of the generalized stiffness matrix $\boldsymbol{K}$ and the generalized mass matrix $\boldsymbol{M}$ of the system are known, taking the coupling characteristics of the matrices $\boldsymbol{M}$ and $\boldsymbol{K}$ into consideration, Equations (3) and (7) are substituted into Equation (1) and expanded for processing, which produces:

$$\begin{bmatrix} M_{11} & M_{15} \\ M_{51} & M_{55} \end{bmatrix} \begin{bmatrix} \ddot{x}_1 \\ \ddot{x}_5 \end{bmatrix} + \begin{bmatrix} K_{11} & K_{15} \\ K_{51} & K_{55} \end{bmatrix} \begin{bmatrix} x_1 \\ x_5 \end{bmatrix} = 0 \tag{8a}$$

$$\begin{bmatrix} M_{22} & M_{24} \\ M_{42} & M_{44} \end{bmatrix} \begin{bmatrix} \ddot{x}_2 \\ \ddot{x}_4 \end{bmatrix} + \begin{bmatrix} K_{22} & K_{24} \\ K_{42} & K_{44} \end{bmatrix} \begin{bmatrix} x_2 \\ x_4 \end{bmatrix} = 0 \tag{8b}$$

$$M_{33}\ddot{x}_3 + K_{33}x_3 = 0 \tag{8c}$$

$$M_{66}\ddot{x}_6 + K_{66}x_6 = 0 \tag{8d}$$

The eigenvalues of Equation (8) are solved respectively; then, the corresponding eigenequations are listed and combined with the parameter characteristics of matrix $\boldsymbol{K}$ and $\boldsymbol{M}$; the following equations can be obtained after sorting:

$$\left(K_{11} - m{\omega_{15}}^2\right)\left(K_{55} - M_{55}{\omega_{15}}^2\right) - \left(K_{15} - {\omega_{15}}^2 M_{15}\right)^2 = 0 \tag{9a}$$

$$\left(K_{22} - m{\omega_{24}}^2\right)\left(K_{44} - M_{44}{\omega_{24}}^2\right) - \left(K_{24} - {\omega_{24}}^2 M_{24}\right)^2 = 0 \tag{9b}$$

$$K_{33} - m{\omega_3}^2 = 0 \tag{9c}$$

$$K_{66} - M_{66}{\omega_6}^2 = 0 \tag{9d}$$

Equation (9a,b) has two eigenvalues, respectively, while Equation (9c,d) has only one eigenvalue. This is due to the fact that the Stewart platform mode has coupling characteristics regarding the X-axis and Y-axis rotation direction but is decoupled regarding the Z-axis.

Theoretically, there are six typical modes of the Stewart platform, including three-order translational modes along the $X/Y/Z$-axes and three-order rotational modes around the $X/Y/Z$-axes [6]. In these six-order modes, the translational mode along the X-axis is coupled with the rotational mode around the Y-axis, which can be reflected in the eigenvalue of Equation (9a). Similarly, the translational mode along the Y-axis is coupled with the rotational mode around the X-axis, which can be reflected in the eigenvalue Equation (9b). In addition, there is no coupling between the translational and rotational modes of the Z-axis and other modes, which is reflected in the eigenvalue of Equation (9c) and (9d), respectively.

The generalized mass matrix $\boldsymbol{M}$ can be obtained by Equation (2). In the case that all elements of matrix $\boldsymbol{M}$ have been determined, if all the 6-order modes of the platform and their corresponding eigenvalues are known, all elements in the generalized stiffness matrix $\boldsymbol{K}$ of the system can be simply obtained by substituting the corresponding eigenvalues of each mode into Equation (9). Finally, according to Equation (4), the additional stiffness matrix $\boldsymbol{K_R}$ of the flexible joint in the Stewart platform can be ultimately solved.

It is worth noting that bringing the eigenvalues into Equation (9a,b) theoretically results in two sets of solutions. This is because, under the same set of eigenvalues, there will be two different modal groups corresponding to them. In this case, the correct solution can be selected by simply solving for the eigenvectors corresponding to the two sets of solutions separately and checking them against the known modes. In addition, $M_{44} = M_{55}$ and $M_{15} = -M_{24}$ should be avoided in the generalized mass matrix $\boldsymbol{M}$, which aims to avoid the unsolvability of Equation (9a,b) being the same, resulting in a system of unsolvable equations. Besides, theoretically, a larger difference in the upper platform and load mass distribution about the X- and Y-axis directions is more capable of ensuring the convergence and accuracy of the solution results.

3. FEM Simulation of Stewart Platform

As an accurate and effective method for the dynamics analysis of complex systems, the finite element method has been well-established in various fields of engineering. Therefore, the FEM simulation was adopted in this paper to solve the modal results of the Stewart platform; the FEM model of the platform is shown in Figure 2. All 6 degrees of freedom of the surface nodes below the Stewart platform are constrained during the process of modal analysis. For determining the stretching stiffness of legs and the bending stiffness of flexible joints in the FEM model of the Stewart platform, the dynamics calibration tests were conducted on the legs and flexible joints, respectively. According to the test results, the relevant material parameters of the leg springs and flexible joints' FEM elements were set and adjusted so that the bending stiffness of the flexible joint in the FEM model is 146.72 N·m/rad, and the axial stretching stiffness of the legs is 324.57 N/mm, which match the test results. It is worth mentioning that the material of the flexible joint is steel, and its FEM model contains only the conventional body elements. After the calibration, the elastic modulus is $E = 184.483$ Gpa, Poisson's ratio is $\mu = 0.3$, and density is $\rho = 7.72792\ \mathrm{kg/mm^3}$. The specific contents of the tests are detailed in Section 4 of this paper and will not be described here.

3.1. FEM Modal Analysis of Stewart Platform

During the establishment of the FEM model, a rectangular mass block was added and fixed to the upper platform of the Stewart platform's FEM model, which aims to enable the difference of the mass distribution existing in the upper platform part between the X and Y axes, the parameters about the mass characteristics of the upper platform with the block can be referred to the Appendix A. In addition, aiming to simplify the analysis process and reduce the error factor, the leg mass was set as 0 in the FEM model.

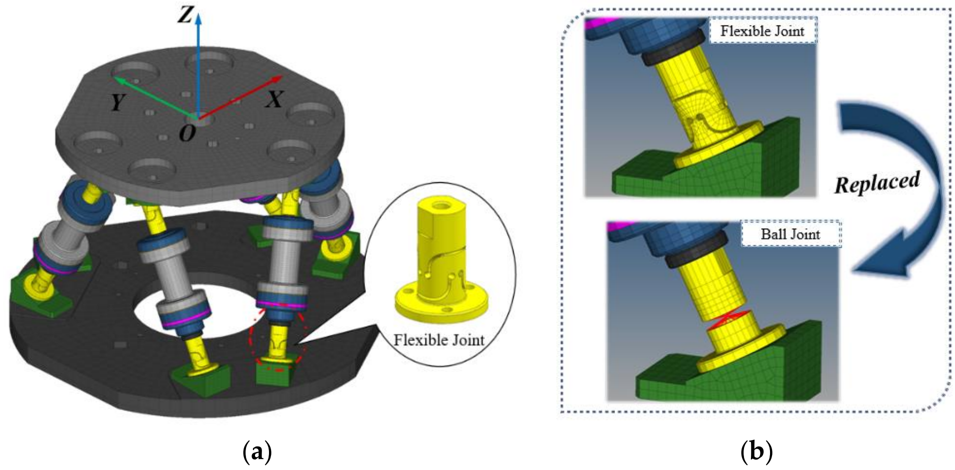

Figure 2. FEM model of the Stewart platform. (**a**) FEM of Stewart platform with flexible joints; (**b**) Equivalent finite element modeling of ball joint.

3.1.1. Modal Analysis of Stewart Platform with Ball Joints

With the purpose of verifying the accuracy of the parameter settings in the FEM model and illustrating the consistency between the FEM simulation and the theoretical calculation results, the flexible joints in the model are first replaced by ball joints without additional stiffness, as shown in Figure 2b, thereby eliminating the additional stiffness effect of the flexible joints on the Stewart platform. In terms of theoretical calculation, the generalized mass matrix $\boldsymbol{M}$ and stiffness matrix $\boldsymbol{K}$ of the system without the influence of the additional stiffness of flexible joints are calculated by Equations (2) and (6), respectively, and then the platform modes can be solved by Equation (1). The Stewart platform modes are solved by theoretical numerical calculation and FEM simulation, respectively, and the modal results obtained are shown in Table 1.

Table 1. Comparison of solved mode results of Stewart platform without flexible joints stiffness.

Mode Form	Modal Eigenvector	Theoretical Natural Frequency/Hz	Simulation Natural Frequency/Hz	Error/%
Translation along the X-axis	$\begin{bmatrix} 1 & 0 & 0 & 0 & -0.965 & 0 \end{bmatrix}^T$	26.21	26.21	−0.03
Translation along the Y-axis	$\begin{bmatrix} 0 & 1 & 0 & 0.833 & 0 & 0 \end{bmatrix}^T$	26.26	26.25	−0.02
Translation along the Z-axis	$\begin{bmatrix} 0 & 0 & 1 & 0 & 0 & 0 \end{bmatrix}^T$	71.62	71.60	−0.03
Rotation around the X-axis	$\begin{bmatrix} 0 & 0.052 & 0 & 1 & 0 & 0 \end{bmatrix}^T$	90.13	88.76	−1.51
Rotation around the Y-axis	$\begin{bmatrix} -0.047 & 0 & 0 & 0 & 1 & 0 \end{bmatrix}^T$	56.42	56.07	−0.61
Rotation around the Z-axis	$\begin{bmatrix} 0 & 0 & 0 & 0 & 0 & 1 \end{bmatrix}^T$	36.88	36.83	−0.14

Table 1 shows that the deviation of natural frequencies obtained by theoretical calculation and simulation is basically consistent. The maximum deviation of natural frequencies corresponding to the three order translational mode is only 0.04%, and the maximum deviation of natural frequency is the one corresponding to the rotational mode around the X-axis, which is just 1.51%. The results can effectively reflect the accuracy of the FEM and the reliability of the modal solution of the FEM method.

3.1.2. Modal Analysis of Stewart Platform with Flexible Joints

On the basis that the high accuracy of the Stewart platform's FEM model has been ensured, the modal solution of the FEM model with flexible joints is further carried out; the modal results are shown in Figure 3.

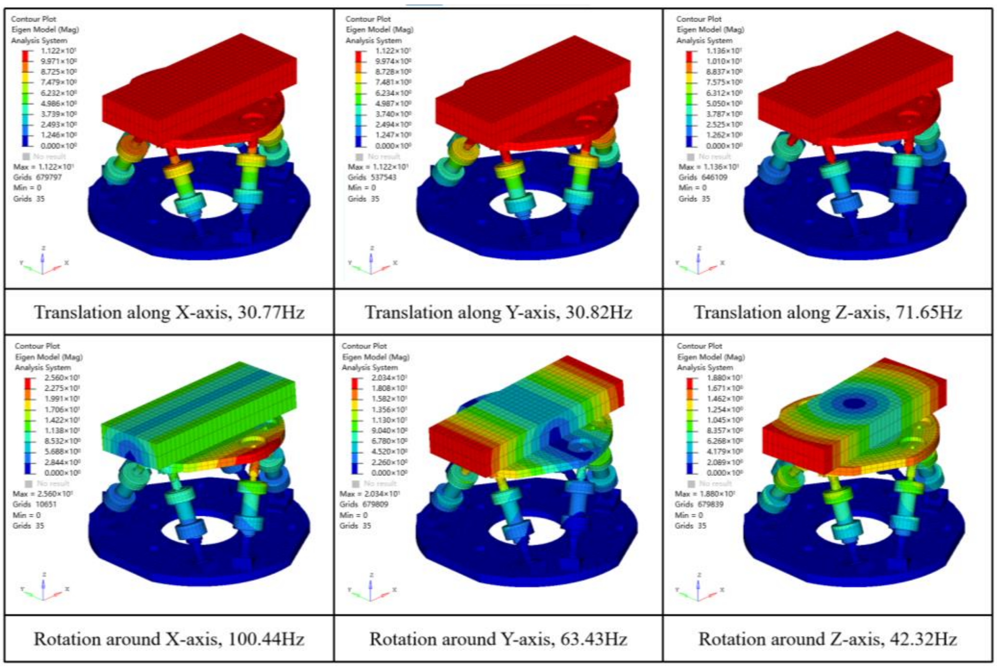

Figure 3. Modal analysis results of Stewart platform with flexible joints.

By substituting the corresponding natural frequencies of each mode in Figure 3 into Equation (9), all parameters in the overall generalized stiffness matrix $\boldsymbol{K}$ of the system can be determined. Based on the solutions of stiffness matrix $\boldsymbol{K}$ and $\boldsymbol{K_S}$, the additional stiffness $\boldsymbol{K_R}$ of the Stewart platform with flexible joints can be obtained by further using Equation (4). Finally, the solved additional stiffness matrix of the Stewart platform with flexible joints is:

$$\boldsymbol{K_R} = 10^4 \times \begin{bmatrix} 7.7319 & 0 & 0 & 0 & -0.6386 & 0 \\ 0 & 7.7319 & 0 & 0.6386 & 0 & 0 \\ 0 & 0 & 0.0646 & 0 & 0 & 0 \\ 0 & 0.6386 & 0 & 0.0831 & 0 & 0 \\ -0.6386 & 0 & 0 & 0 & 0.0831 & 0 \\ 0 & 0 & 0 & 0 & 0 & 0.1108 \end{bmatrix} \tag{10}$$

3.2. Verification of Solving Results for Additional Stiffness of Flexible Joints

Further simulations are prepared around the Stewart platform in this paper based on the stiffness matrix $\boldsymbol{K_s}$ obtained to verify the correctness of the theoretical method. In order to accomplish this, the following method is adopted in this paper: maintaining the stiffness characteristics of the flexible joints in the Stewart platform, the mass characteristics of the system and stretching stiffness values of legs are changed, and then the modal solution of the platform system under different mass states are calculation separately by theoretical numerical and FEM approach. Afterward, the accuracy of the solved $\boldsymbol{K_s}$ can be verified by comparing the theoretical and simulation results. The specific conditions of characteristic change selected in this paper are:

(a) The mass of the rectangular load is changed to twice the original mass, and the leg stretching stiffness is changed to 1.5 times the original.
(b) The rectangular load of the upper platform is removed, and the corresponding mass characteristics of the legs are attached.

The corresponding modal results were respectively obtained after the FEM simulations. The modal results of condition (a) are basically similar to Figure 3 and are not shown here to save space. The modal results corresponding to condition (b) are shown in Figure 4.

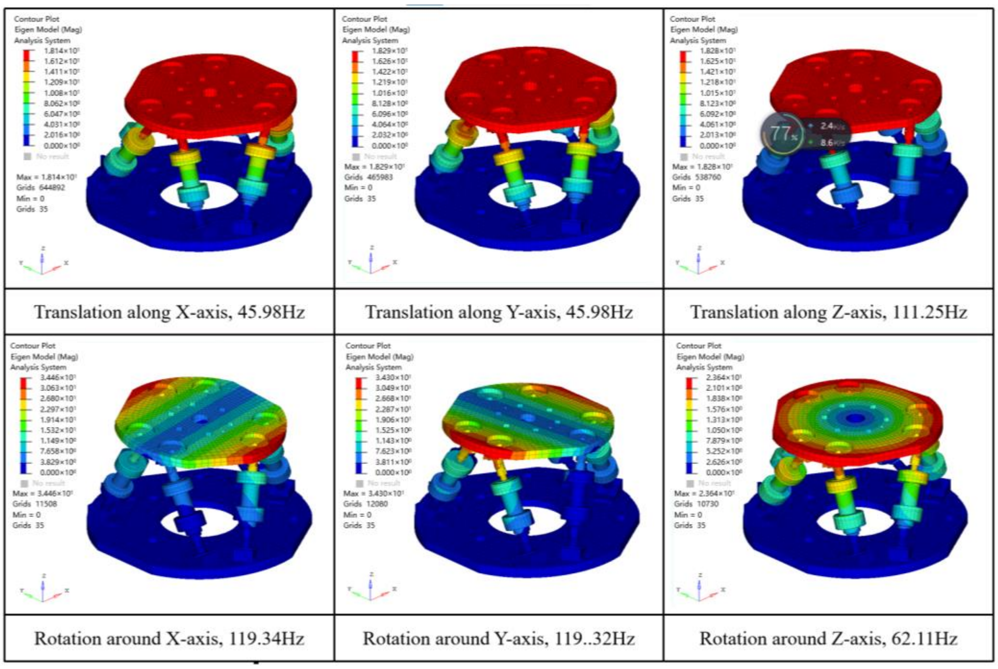

Figure 4. Modal analysis results of the Stewart platform prototype.

It is worth noting that the main purpose of condition (b) is to correspond to the actual dynamic conditions of the Stewart platform for testing. The relevant parameters involved in the process are given in Appendix A and are omitted here. The ultimate calculation results are shown in Table 2.

Table 2. Comparison of solved mode of Stewart platform without flexible joints stiffness.

Mode Form	Condition (a)			Condition (b)		
	Theoretical Natural Frequency/Hz	**Simulation Natural Frequency/Hz**	**Error/%**	**Theoretical Natural Frequency/Hz**	**Simulation Natural Frequency/Hz**	**Error/%**
Translation along the X-axis	28.04	27.93	−0.39	45.96	45.98	0.03
Translation along the Y-axis	28.06	27.93	−0.44	45.96	45.98	0.03
Translation along the Z-axis	68.02	67.67	−0.51	110.29	111.25	0.87
Rotation around the X-axis	102.54	100.23	−2.26	119.43	119.34	−0.07
Rotation around the Y-axis	56.68	56.26	−0.75	119.45	119.32	−0.11
Rotation around the Z-axis	38.47	38.30	−0.45	62.39	62.11	−0.44

As can be seen in Table 2, the maximum deviation between the natural frequency results separately calculated by theory and FEM simulation under condition (a) is 2.26%, while the maximum deviation under condition (b) is just 0.87%. By comparing the natural frequency results under the characteristic conditions, the effectiveness of the proposed method for solving the additional stiffness of flexible joints can be verified.

4. Dynamics Tests of Stewart Platform

4.1. Overview of Stewart Platform

The main body of the Stewart platform is composed of an upper platform, a lower platform and six parallel outrigger legs. The upper and lower platforms are connected to the legs by flexible joints. Through the platform structural parameters detection and error analysis, the position accuracy of theoretical joint points of the platform is better than 0.2 mm. After the error theory calculation, the overall stiffness of the platform system caused by the platform structure size error is less than 2.5%, which meets the test's accuracy requirements. The relevant platform parameters are detailed in the attached table.

4.2. Calibration Tests for Stiffness of Legs and Flexible Joints

During the operation of the Stewart platform, the movement stroke of the upper platform is relatively small, the telescopic deformation of the leg is less than 1 mm, and the bending deformation of the elastic joint is less than 1°. Therefore, the dynamics method of stiffness testing and calibration was adapted so that more accurate measurements of the stiffness under small deformations of the flexible components could be obtained. The schematic diagram of the tests is shown in Figure 5. Here, the stretching stiffness of the legs and the bending stiffness of the flexible joints are considered single-degree-of-freedom linear stiffnesses, so they are equivalent to the spring-mass system during the tests.

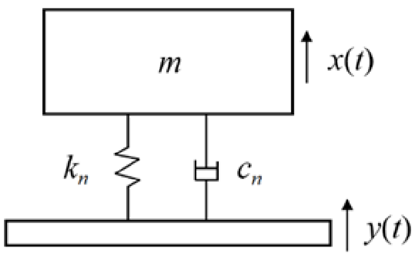

Figure 5. Schematic diagram of stiffness calibration test.

Since the damping in the system is relatively small, which reflects from the frequency response curves tested following, after neglecting its effect, the system's natural frequency can be obtained as:

$$f_n = \frac{1}{2\pi}\sqrt{\frac{k_n}{m_n}} \tag{11}$$

where, k_n denotes the stiffness of the flexible component to be measured, and m_n denotes the load mass. When the natural frequency f_n and load mass m_n of the system are known, the stiffness to be measured k_n can be easily calculated according to Equation (11).

The tests were conducted in the form of a frequency response test, and the frequencies corresponding to the peaks of the frequency response curves were measured to determine the natural frequencies of the system. During the tests, the legs and flexible joints were respectively placed on the vertical and horizontal vibration platforms, as shown in Figure 6. In the process of testing, when a flexible joint was tested, a mass block was installed above the joint as the load, and when a leg was tested, the leg itself was treated as the load. The excitation is in the form of sinusoidal acceleration with an amplitude of 0.1 g and a frequency range of 10~300 Hz. The test excitation table, code-named DC-6500-65, was manufactured by STI (Sushi Testing Instruments Co., Suzhou, China). Its rated operating frequency range is 2–2700 Hz, and the maximum error of its output acceleration is about ±10% under the test conditions in this paper. The tested sensors are three-way acceleration sensors produced by PCB PIEZOTRONICS (Buffalo, NY, USA), model 356A33, with a sensitivity of about 10.32 mV/g and an error of less than ±0.3% at 0–1000 Hz.

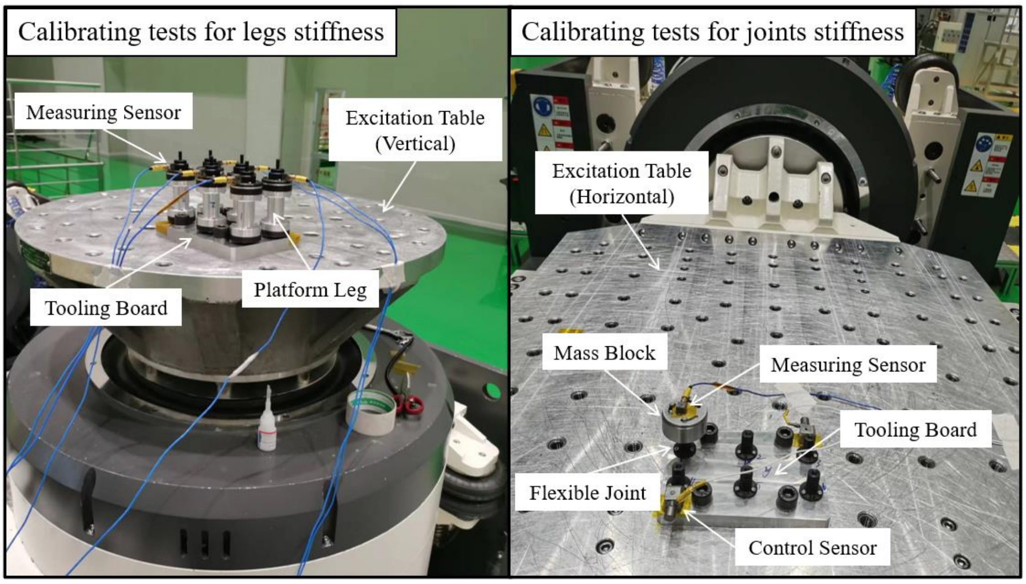

Figure 6. Stiffness calibration test of flexible components.

The frequency response curves and the corresponding peak frequencies of the legs and flexible joints measured through the tests are given in Figure 7:

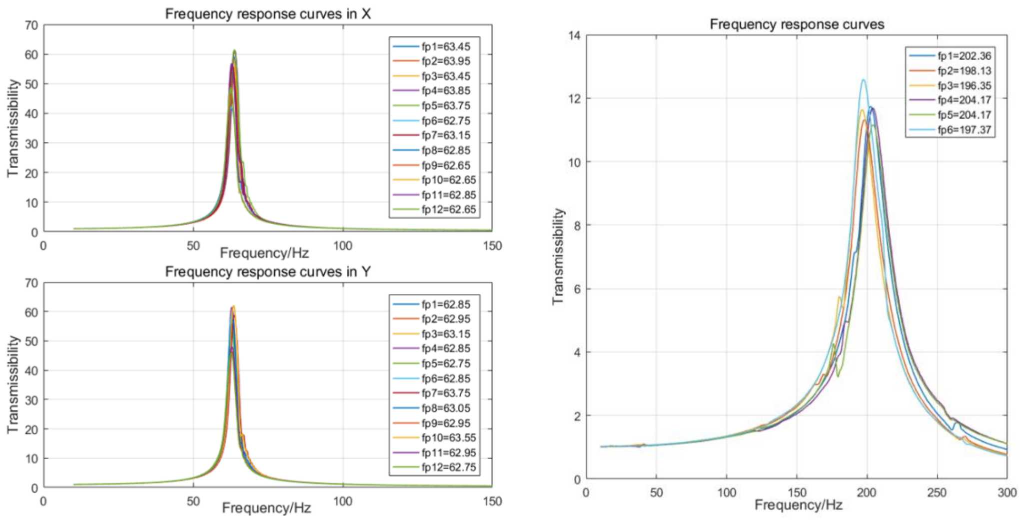

Figure 7. Frequency response curves obtained from flexible components tests: (**a**) Frequency response curves of flexible joints; (**b**) Frequency response curves of legs.

The stretching stiffness of the outrigger legs and the bending stiffness of the flexible joints are finally calculated through Equation (11). As shown in Table 3, both the stretching stiffness of the legs and the bending stiffness of the flexible joints have a good consistency. Therefore, for more intuitive theoretical analysis, the average value is taken for calculation in the paper. After averaging, the stretching stiffness of the legs equals 324.57 N/mm, and the bending stiffness of flexible joints equals 146.72 N·m/rad.

Table 3. Stiffness values of flexible components obtained from the tests.

Stretching stiffness of legs												
	1		2		3		4		5		6	
Stretching along axial direction (N/mm)	330.78		317.11		311.42		336.72		336.72		314.67	
Bending stiffness of flexible joints												
	1	2	3	4	5	6	7	8	9	10	11	12
Bending around the X-direction (N·m/rad)	148.0	150.3	148.0	149.9	149.4	144.8	146.7	145.2	144.4	144.3	145.2	144.5
Bending around the Y-direction (N·m/rad)	145.9	146.3	147.2	145.9	145.4	145.9	150.0	146.7	146.4	149.1	146.3	145.4

4.3. Frequency Response Tests of Stewart Platform

Stewart platform dynamics tests adopt the form of a frequency response test so that the frequency response curves of the platform system can be measured, and then the low-order natural frequencies of the platform system can be found by observing the corresponding peaks of the curves. During the tests, the Stewart platform was placed on the excitation table, and the lower platform was fixed to the excitation table, as shown in Figure 8. The sensors were selected as accelerometers, the control sensor was attached to the surface of the lower platform, and the measurement sensor was attached to the upper platform near the center. The definition of the test coordinate system was the same as that of the platform coordinate system. The Stewart platform was successively loaded with vibration excitation in $X/Y/Z$ directions, and the excitation occured in the form of sinusoidal acceleration with an amplitude of 0.1 g and a frequency range of 10~500 Hz.

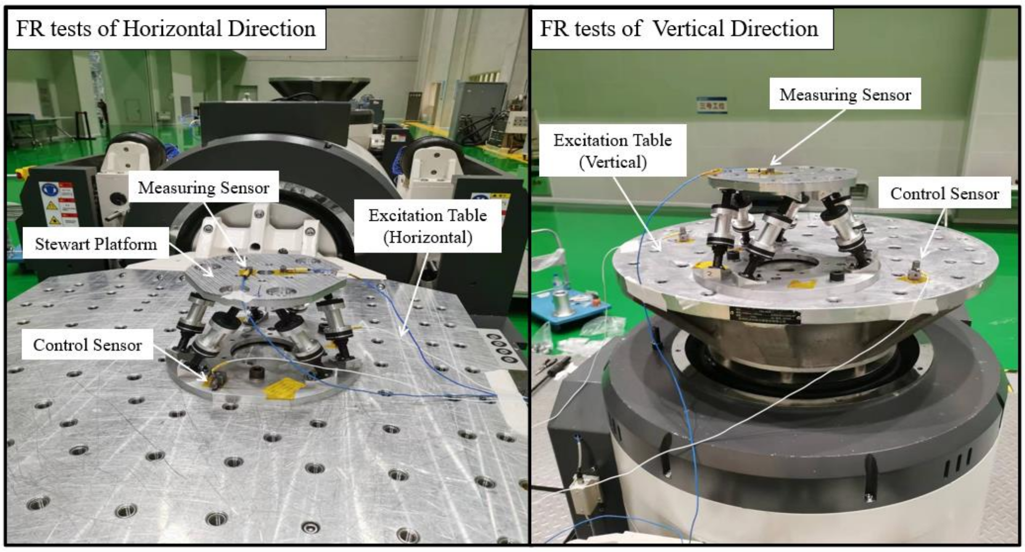

Figure 8. Frequency response tests of Stewart platform.

The frequency response curves measured by the tests are shown in Figure 9. As can be seen from the figure, there are two resonance peaks in the X-direction frequency response curve, which respectively correspond to the translational mode of the Stewart platform along the X-axis and the rotational mode around the Y-axis; this indicates the coupling characteristics of the system regarding the X-direction and Y-direction, which conforms to the theory and is similar for the Y-direction frequency response curve. The Z-direction frequency response curve in the figure has only one resonance peak, which corresponds to the translational mode of the system along the Z-axis, indicating that there is no coupling characteristic with respect to the Z-direction. In addition, the high consistency of the

X-direction and Y-direction frequency response curves reflects not only the symmetry characteristics of the Stewart platform but also the high manufacturing accuracy of the platform, which indirectly affirms the credibility of the tests.

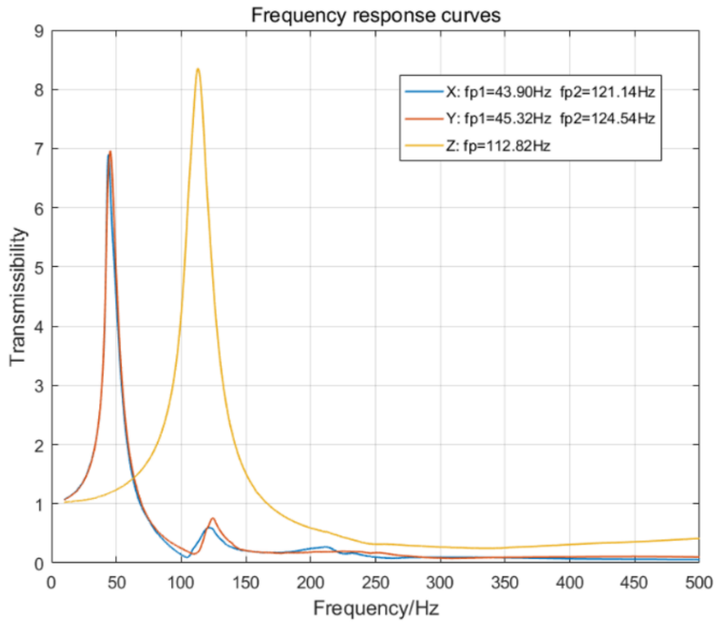

Figure 9. Frequency response test results of Stewart platform.

The natural frequencies of the system corresponding to the translational modes of the Stewart platform along the three directions of $X/Y/Z$ axes and the rotational modes around the X/Y axes are extracted from Figure 9. After further comparison with the result with the theoretical natural frequency of the platform in Section 3.2, the final compiled results are presented in Table 4.

Table 4. Comparison between Stewart platform test and natural frequency.

Modal Characteristics	Theoretical Natural Frequency/Hz	Test Natural Frequency/Hz	Error/%
Moving along the X-axis	45.96	43.90	−4.48
Moving along the Y-axis	45.96	45.32	−1.39
Moving along the Z-axis	110.29	112.82	2.29
Rotating along the X-axis	119.43	124.54	4.28
Rotating along the Y-axis	119.45	121.140	1.41
Rotating along the Z-axis	62.39	-	-

Due to the inability of the excitation platform to generate the torque form of excitation and that there is no coupling between the rotational mode of the platform around the Z-axis direction and other modes, the corresponding natural frequency of the mode cannot be obtained from the tests. Nevertheless, from the other fifth-order mode corresponding to the natural frequency in Table 4, it can still be seen that the maximum error of the experimental natural frequency results does not exceed 5% compared to the theoretical calculations, which are comparable to the theoretical results. The accuracy and reliability of the proposed method for the additional stiffness of Stewart platform flexible joints are further verified through actual testing of the natural frequency of the Stewart platform.

5. Discussion

5.1. Additional Illustration of the Theoretical Method

It is observed from the previous contents that the method proposed in this paper reasonably depends on the symmetry of the Stewart configuration mechanism. Due to the structural axis-symmetric characteristics of the vertical Z-axis, the dynamics of the mechanism exhibit theoretical consistency in the horizontal X and Y directions, which is particularly reflected in the generalized stiffness matrix K of the system. In addition, the mechanism exhibits the same symmetry characteristics regarding the dynamical coupling of both the X and Y axes. In many past studies, it can be found that the traditional type of Stewart configuration mechanism almost always has such properties of symmetry, and their stiffness matrix has the same parameter characteristics as Equation (7). Whenever this condition is satisfied, the solution of the additional stiffness of the flexible joint can be accomplished according to the theoretical method of this paper. According to the traditional kinematic theoretical method, it is inevitable to conduct different forms of kinematic analysis and theoretical derivation for the additional stiffness that exists in Stewart mechanisms with different types and distributions of flexible joints, and the derivation results can only be applied to one type of Stewart mechanism. In contrast, the method in this paper is more applicable and feasible for solving the additional stiffness of flexible joints in various forms of the Stewart mechanism. In addition, the theoretical idea of this paper can also be applied to the generalized Stewart mechanism mentioned by Jiang [36], which contains a more complicated coupling relationship of stiffness characteristics compared to the traditional Stewart mechanism, including translational stiffness along the X-axis and rotation stiffness around the X-axis, translational stiffness along the Y-axis and rotation stiffness around the Y-axis, and translational stiffness along the Z-axis and rotation stiffness around the Z-axis. The generalized stiffness matrix of the system corresponding to the mechanism follows the equation:

$$\boldsymbol{K_G} = \begin{bmatrix} K_{11} & 0 & 0 & K_{14} & K_{15} & 0 \\ 0 & K_{22} & 0 & K_{24} & K_{25} & 0 \\ 0 & 0 & K_{33} & 0 & 0 & K_{36} \\ K_{41} & K_{42} & 0 & K_{44} & 0 & 0 \\ K_{51} & K_{52} & 0 & 0 & K_{55} & 0 \\ 0 & 0 & K_{63} & 0 & 0 & K_{66} \end{bmatrix} \tag{12}$$

where, apart from the same parameter characteristics as in Equation (7), the elements satisfy: $M_{14} = M_{25} = M_{41} = M_{52}$. This shows that there are two more values to be solved in the matrix $\boldsymbol{K_G}$ compared to the stiffness matrix K, which means there are seven parameters to be solved in the matrix $\boldsymbol{K_G}$. However, the Stewart platform dynamics equations have only six modal solutions, which can only provide six eigenequations, which makes the set of equations unsolvable. The method given by the authors here follows. Before the step of the FEM modal solution for the Stewart platform, the upper platform shall be added to two different mass blocks successively and conducts the modal solution so that more eigenvalues and eigenequations can be obtained. Then the solution can be achieved when the number of eigenequations is more than that of solving parameters in fo matrix $\boldsymbol{K_G}$. Although the usage of the method proposed for the generalized Stewart mechanism is more complicated than that of the traditional Stewart mechanism, it is still quite acceptable compared to the theoretical kinematic method with respect to the increased difficulty. The relevant content of this has not been studied deeply in the paper, and readers are encouraged to try it out.

Although the objective of the method in this paper is to find the additional stiffness induced by the flexible joints in the Stewart mechanism, the method proposed is essentially a solution for the overall stiffness of the system with the flexible joints. For conformity with the actual engineering situation and better illustration, the solution to the additional stiffness caused by the flexible joints in this paper is based on the premise that the generalized stiffness caused by the legs in the system is known. In fact, if the system stiffness caused by the legs is unknown, the additional stiffness caused by the flexible joint in the system can also be solved directly by setting the axial stretching stiffness of the legs in the FEM model to zero and keeping the flexible joint stiffness in the system. In practical situations, Stewart mechanisms may contain more than one type of flexible joint (e.g., bending-deformed flexible joints, torsion-deformed flexible joints). In this case, it is rather challenging to achieve a kinematic theoretical derivation to solve selectively for the additional stiffness caused by one or several groups of flexible joints in the system. However, it can be achieved straightforwardly by the method proposed, in which the corresponding stiffness of the irrelevant flexible components in the FEM model just needs to be set to zero before determining the FEM modal solution. Then the additional stiffness caused by the specified flexible joints can be obtained by bringing the obtained eigenvalues into the corresponding eigenequations to solve.

Furthermore, there are two issues need to be mentioned: 1. Since the method in this paper relies on the FEM modal solution results, a relatively good consistency between the established FEM model and the corresponding parameters in the set of eigenequations needs to be ensured, which determines the accuracy of the solution results. 2. During the process of adding additional load to the upper platform, it should be ensured that the overall mass distribution of the upper platform has differences in the X-axis and Y-axis directions to avoid the situation that $M_{44} = M_{55}$ and $M_{15} = -M_{24}$ in the matrix $\boldsymbol{M}$, thus preventing the situation that the characteristic Equation (9a,b) is the same without solutions. Moreover, theoretically, the greater the difference between the upper platform part's mass distribution about the X-axis and Y-axis directions, the better convergence and accuracy of the solution results can be obtained.

5.2. Damping Effects Analysis of Stewart Platform

The theoretical method proposed in this paper is primarily based on the modal analysis for the system stiffness solution, so the damping characteristics of the system are not considered during the theoretical analysis. However, during the actual tests, the dynamics behavior of the Stewart platform prototype will inevitably be affected by damping. For further clarification of the reasonableness of the test results under the influence of damping, the analysis and discussion around the influence of system damping follow.

Firstly, it should be specified that the Stewart platform tested adopts a gapless structure design, and the movements between the platform components depend on the elastic deformation of the flexible components (legs and hinges), which causes no frictional damping to occur in the system. Therefore, here we mainly consider the damping from the elastic deformation of the legs and the flexible joints, which is the main source of the damping compared to the structural damping and the air damping during the tests. Here, we temporarily assume linear damping; the specific values can be calculated using Equation (A2) in Appendix A and the frequency response curves obtained from the tests in Section 4.2. Then, the damping matrices of the system corresponding to the legs and the flexible joints are sequentially calculated by relevant dynamics theory, and the results are referred to in Appendix A. Based on this, the dynamics equation of the system under unit sinusoidal excitation [6] is given as follows:

$$\boldsymbol{M}\ddot{\boldsymbol{X}} + n\boldsymbol{C}\dot{\boldsymbol{X}} + \boldsymbol{K}\boldsymbol{X} = n\boldsymbol{C}\dot{\boldsymbol{Y}} + \boldsymbol{K}\boldsymbol{Y} \tag{13}$$

where $\boldsymbol{C}$ denotes the system damping matrix, and given that the displacement of the payload platform is $\boldsymbol{X}$, and the displacement of the base platform is $\boldsymbol{Y}$ when a sinusoidal excitation is applied to the base platform, and the displacement of the base platform is: $\boldsymbol{Y} = \begin{bmatrix} Y_1 & Y_2 & Y_3 & Y_4 & Y_5 & Y_6 \end{bmatrix}^T$. Here, $Y_i = y_i sin\omega t\ (i = 1 \sim 6)$. Besides, the damping multiplication factor n is multiplied ahead of the damping matrix $\boldsymbol{C}$. By changing the magnitude of n and solving Equation (13) sequentially, the frequency response curve of the Stewart platform with different damping can be obtained; the results are shown in Figure 10.

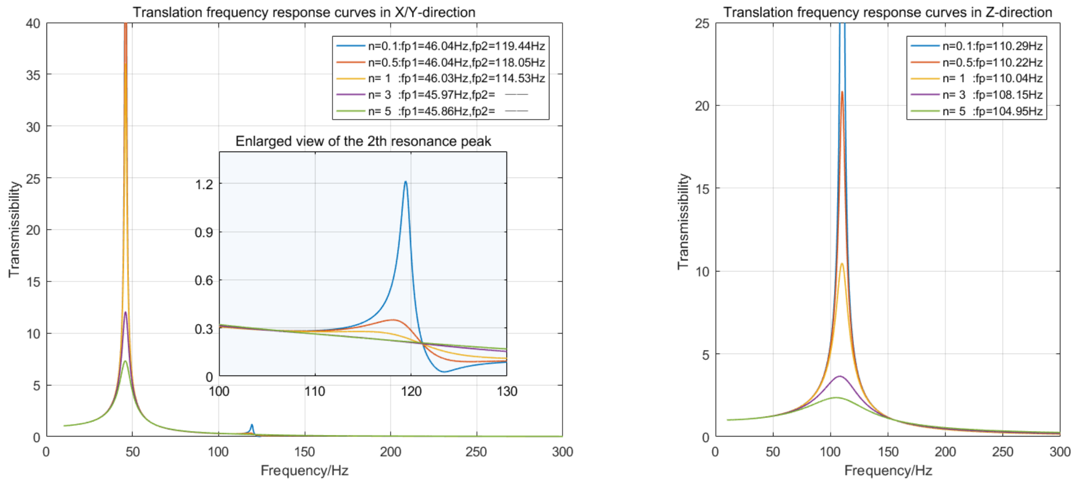

(**a**) (**b**)

Figure 10. Stewart platform frequency response curves with different damping: (**a**) horizontal X/Y-direction frequency response curves; (**b**) vertical Z-direction frequency response curves.

After compilation, the natural frequencies of the Stewart platform with different damping are shown in Table 5:

Table 5. Theoretical natural frequencies of Stewart platform with different magnification damping.

Damping Amplification n	*X/Y*-Direction First-Order Natural Frequency/Hz	*X/Y*-Direction Second-Order Natural Frequency/Hz	*Z*-Direction First-Order Natural Frequency/Hz
0.1	46.04	119.44	110.29
0.5	46.04	118.05	110.22
1	46.03	114.53	110.04
3	45.97	-	108.15
5	45.86	-	104.95

Figure 10 and Table 5 show that the Stewart platform resonance peak decreases as the damping of the system increases, and the X/Y-direction second-order resonance peak disappears when the damping increases to a certain level. Meanwhile, the natural frequencies of each order of the system have different degrees of decline, in which the first-order natural frequency of X/Y direction with lower frequency has little change, and the second-order natural frequencies of X/Y direction and Z direction with higher frequency have larger changes. Considering that the first-order natural frequencies of X/Y directions obtained from the tests are in strong agreement with the theoretical results, it can be considered that the first-order natural frequencies of the Stewart platform prototype in the tests are less affected by damping, and the negligence of the damping effect in the tests is justified to some extent.

Furthermore, we can observe that there is a large error in the higher X/Y-direction second-order natural frequencies and Z-direction natural frequency under the assumption of linear damping. For this phenomenon, the authors give the following explanation after analysis. First, the curves in Figure 10 are obtained under the premise that the damping of the system remains constant throughout the tests, but further observation shows that the actual second-order peak of the system is larger than the theoretical calculation, and the relatively first-order peak is significantly smaller than the theoretical result, so it can be concluded that the damping of the system during the second-order resonance is relatively smaller than that during the first-order resonance. Therefore, the actual second-order natural frequency is much closer to the theoretical natural frequency of 119 Hz without damping, which indicates that the actual effect of damping on the second-order natural frequency of the system is obviously smaller. If so, a new problem arises here, the theoretical

Z-directional resonance amplitude is close to the test results, and the Z-directional natural frequency is near the X/Y-directional second-order natural frequency, which contradicts the conclusion that the damping coefficient decreases in the high-frequency area. The authors speculate that it is due to the energy loss caused by the large-amplitude vibration of the system during the vibration process, which can also be confirmed by the fact that the theoretical X/Y first-order resonance amplitude is significantly larger compared to the test results. It is worth mentioning that the Stewart platform legs are equipped with damping components manufactured from viscoelastic materials, and the damping components may produce small creep on the surface of the closely attached parts while deforming during the system motion. Therefore, the author considers that the use of viscoelastic materials causes the complex damping characteristics of the system.

According to the theoretical analysis, the system-damping effect mainly acts in the higher frequency band. Under the assumption of constant damping in the full frequency band, the test error for the higher frequency X/Y-direction second-order natural frequency and Z-direction natural frequency is around 8%. However, the analysis of the test results shows that the damping in the high-frequency band is significantly lower than that in the low-frequency band, which entails that the damping-induced natural frequency error in the high-frequency band during the tests could be less than 8%. Therefore, the premise of the negligence of the damping effect can still be considered reasonable. Although the system damping has a certain influence on the test results, the overall correctness of the theoretical method of this paper can still be confirmed by the tests.

6. Conclusions

In this paper, combining the symmetry characteristics of the Stewart mechanism with relevant dynamics theory as a method of solving the additional stiffness of flexible hinges in the Stewart mechanism based on FEM modal analysis is proposed. Following the proposed method, the additional stiffness caused by the flexible joints has been solved for the developed Stewart platform. Furthermore, the method is systematically validated from simulations and tests based on the solution results. In the simulation process, the modal solution of the Stewart platform was conducted under specific conditions separately by numerical calculation and FEM simulation. The comparison of the two sets of results shows that the typical natural frequencies of the system obtained by the two approaches are close to each other, with a maximum deviation of only 3.12%, which verifies the correctness of the theoretical method proposed in this paper. The frequency response test was conducted on the Stewart platform prototype, and the natural frequencies of the typical modes were extracted from the frequency response curves obtained from the tests. By comparing with the theoretical results, it indicates that the maximum error between the actual natural frequency of the platform prototype and the theoretical calculation results does not exceed 5%, which proves the effectiveness of the proposed method for solving the additional stiffness of the flexible joints in practical engineering applications. Through combining the test results with the dynamics theory, further analysis and discussion are conducted around the influence of system damping on the test results, which indicates that the damping effect on the natural frequencies of the tested Stewart platform is within acceptable limits, and the tests still have a high degree of reliability. The research of this paper provides a certain technical reference for the application and design of the Stewart platform with flexible joints.

Author Contributions: Conceptualization, T.Z. and X.G.; methodology, T.Z. and Y.L.; software, T.Z.; validation, T.Z. and Y.W.; formal analysis, T.Z.; investigation, T.Z. and Y.W.; resources, L.Z.; data curation, T.Z.; writing—original draft preparation, T.Z.; writing—review and editing, T.Z., Y.W., X.G. and L.L.; visualization, T.Z.; supervision, L.Z.; project administration, L.Z.; funding acquisition, L.Z. and L.L. All authors have read and agreed to the published version of the manuscript.

Funding: This research was funded by: 1. Scientific and Technological Developing project of Ji Lin Province, No. 20210509052RQ; 2. National Natural Science Foundation of China, No. 52275083.

Data Availability Statement: Not applicable.

Acknowledgments: The authors would like to acknowledge the contribution of all authors of this paper, the technical support from Chang Guang Satellite Technology Co., Ltd., and the funding from the Scientific and Technological Developing Project of Ji Lin Province and National Natural Science Foundation of China. Moreover, the authors thank the editors and reviewers for their time and effort in reviewing this paper.

Conflicts of Interest: The authors declare no conflict of interest.

Appendix A

The main parameters of the Stewart platform used for simulation and experiment in this paper are shown in Table A1, which are also supported by the relevant theoretical analysis and calculation in this paper.

Table A1. Main parameters of Stewart platform.

Parameter	Value
Upper platform joint point circle radius R_P	100 mm
Lower platform joint point circle radius R_B	140 mm
Distribution angle of upper platform joint points α	40°
Distribution angle of lower platform joint points β	30°
Height between the upper and lower point circles H	124 mm
Coordinates of the load centroid in coordinate system O_P-XYZ	[0, 0, 30.12] mm
Distance from upper centroid of leg to upper joint point l_{sp}	47.600 mm
Distance from lower centroid of leg to lower joint point l_{sb}	62.795 mm
Load mass of upper platform m	2.574 kg
Load inertia tensor relative to the centroid I	[10,983, 10,976, 21,586] kg·mm^2
Mass of upper part of the leg m_{sp}	0.09387 kg
Mass of lower part of the leg m_{sb}	0.41013 kg
The upper part inertia tensor of leg relative to the centroid I_{sp}	[77.15, 77.15, 5.03] kg·mm^2
The lower part inertia tensor of leg relative to the centroid I_{sb}	[522.21, 522.21, 99.16] kg·mm^2

In Section 3.1, to avoid the complete symmetry of the mass characteristics of the upper platform of the Stewart platform, the rectangular load is attached to the upper platform. Besides, for the verification of the correctness of the solved additional stiffness of the flexible joints, the mass of the load is set to 1.5 times the original in Section 3.2. Table A2 shows the mass characteristic parameters of the upper platform and its load under different conditions.

Table A2. The parameters of load and upper platform mass characteristics.

Description of Platform and Load	Mass/kg	Moment of Inertia Relative to the Centroid/kg·mm^2	The Coordinates of the Centroid in Coordinate System O_P-XYZ/mm
No load	2.542	$\begin{bmatrix}10,810.80 & 10,816.31 & 21,256.41\end{bmatrix}$	$\begin{bmatrix}0 & 0 & 30.116\end{bmatrix}$
Loaded	7.542	$\begin{bmatrix}20,145.31 & 51,650.40 & 64,755.82\end{bmatrix}$	$\begin{bmatrix}0 & 0 & 54.567\end{bmatrix}$
Load mass (×1.5)	12.5446	$\begin{bmatrix}27,651.70 & 90,656.36 & 108,255.23\end{bmatrix}$	$\begin{bmatrix}0 & 0 & 59.523\end{bmatrix}$

When considering the outrigger legs masses in condition (b) of Section 3.2, based on the system generalized mass matrix $\boldsymbol{M}$ in the dynamics Equation (1), there is a need to add an additional generalized mass matrix of the legs $\boldsymbol{M_L}$, which is already given below:

$$\boldsymbol{M_L} = \sum_{i=0}^{6} {}^{P}\boldsymbol{J}_i^{T}(\boldsymbol{M_1} + \boldsymbol{M_2})_i {}^{P}\boldsymbol{J}_i \quad \text{(A1)}$$

where:

$$\boldsymbol{M_1} = \left(\boldsymbol{E_3} + \frac{l_{sp}\widetilde{\boldsymbol{n}}_{\boldsymbol{i}}^{\boldsymbol{2}}}{l_i}\right)^T m_{sp}\left(\boldsymbol{E_3} + \frac{\boldsymbol{l_{sp}}\widetilde{\boldsymbol{n}}_{\boldsymbol{i}}^{\boldsymbol{2}}}{l_i}\right) + \frac{m_{sb}l_{sb}^2\widetilde{\boldsymbol{n}}_{\boldsymbol{i}}^{\boldsymbol{T}}\widetilde{n}_i}{l_i^2}$$

$$\boldsymbol{M_2} = \left(\boldsymbol{I_{sp}} + \boldsymbol{I_{sb}}\right)\frac{\widetilde{\boldsymbol{n}}_{\boldsymbol{i}}^{\boldsymbol{T}}\widetilde{\boldsymbol{n}}_{\boldsymbol{i}}}{l_i^2}$$

$${}^{P}\boldsymbol{J_i} = \left[\boldsymbol{E_3} \quad (\boldsymbol{R}\cdot\boldsymbol{P_i} \times \boldsymbol{E_3})\right]$$

where $\boldsymbol{n_i}$ denotes the unit vector of the i-th leg; l_i denotes the length of the i-th leg; $\boldsymbol{E_3}$ is the third-order identity matrix; $\boldsymbol{R}$ is the coordinate transformation matrix between the coordinate system O_P-XYZ and O_B-XYZ; $\boldsymbol{P_i}$ denotes the coordinate of the upper joint point of the i-th leg in the coordinate system O_P-XYZ; The corresponding values of specific parameters can be found in Table A1.

For the dynamic calibration tests of the legs and flexible joints, the test system was equated to a single-degree-of-freedom linear spring-mass system; the schematic is shown in Figure 4. Through the dynamics theoretical derivation, the peak value of the system frequency response curve P_n and its corresponding frequency f_n^P can be respectively obtained as:

$$P_n = \frac{1}{2\xi\sqrt{1-\xi^2}} \tag{A2a}$$

$$f_n^P = \sqrt{(1-2\xi^2)\frac{\mathrm{k}}{m}} \tag{A2b}$$

where $\xi = \frac{c_n}{2\sqrt{k_n m_n}}$, c_n denotes the linear damping of the testing object. The test results of all tested legs and flexible hinges are calculated separately and then averaged, and the corresponding damping matrices of the legs and flexible hinges in the Stewart platform are finally obtained after derivation as follows:

$$\boldsymbol{C_S} = \begin{bmatrix} 7.7319 & 0 & 0 & 0 & -0.6386 & 0 \\ 0 & 7.7319 & 0 & 0.6386 & 0 & 0 \\ 0 & 0 & 0.0646 & 0 & 0 & 0 \\ 0 & 0.6386 & 0 & 0.0831 & 0 & 0 \\ -0.6386 & 0 & 0 & 0 & 0.0831 & 0 \\ 0 & 0 & 0 & 0 & 0 & 0.1108 \end{bmatrix} \tag{A3a}$$

$$\boldsymbol{C_R} = \begin{bmatrix} 29.0905 & 0 & 0 & 0 & 2.2961 & 0 \\ 0 & 29.0905 & 0 & -2.2961 & 0 & 0 \\ 0 & 0 & 211.8189 & 0 & 0 & 0 \\ 0 & -2.2961 & 0 & 1.0591 & 0 & 0 \\ 2.2961 & 0 & 0 & 0 & 1.0591 & 0 \\ 0 & 0 & 0 & 0 & 0 & 0.4823 \end{bmatrix} \tag{A3b}$$

The damping of the system introduced by the legs and flexible hinges in the Stewart platform is: $\boldsymbol{C} = \boldsymbol{C_S} + \boldsymbol{C_R}$.

References

1. Gough, V.E. Contribution to discussion of papers on research in automobile stability, control and tyre performance. *Proc. Automot. Div. Inst. Mech. Eng.* **1957**, *171*, 392–395.
2. Furqan, M.; Suhaib, M.; Ahmad, N. Studies on Stewart platform manipulator: A review. *J. Mech. Sci. Technol.* **2017**, *31*, 4459–4470. [CrossRef]
3. Dragne, C.; Chiroiu, V. Gough-Stewart Platform Stiffness and Eigenmodes Evaluation. In Proceedings of the Acoustics and Vibration of Mechanical Structures—AVMS-2021: Proceedings of the 16th AVMS, Timişoara, Romania, 28–29 May 2021; Springer International Publishing: Cham, Switzerland, 2022; pp. 319–328.
4. He, Z.; Feng, X.; Zhu, Y.; Yu, Z.; Li, Z.; Zhang, Y.; Wang, Y.; Wang, P.; Zhao, L. Progress of Stewart Vibration Platform in Aerospace Micro-Vibration Control. *Aerospace* **2022**, *9*, 324. [CrossRef]

5. Kizir, S.; Bingül, Z. Design and development of a Stewart platform assisted and navigated transsphenoidal surgery. *Turk. J. Electr. Eng. Comput. Sci.* **2019**, *27*, 961–972. [CrossRef]
6. Zhang, T.; Gong, X.; Zhang, L.; Yu, Y. A New Modeling Approach for Parameter Design of Stewart Vibration Isolation System Integrated into Complex Systems. *Machines* **2022**, *10*, 1005. [CrossRef]
7. Zhao, Y.; Cao, Y.; Zhang, C.; Zhang, D.; Zhang, J. Error modeling and experimental study of a flexible joint 6-UPUR parallel six-axis force sensor. *Sensors* **2017**, *17*, 2238. [CrossRef]
8. Wang, P.P.; Liu, L.; Qian, Q.R. Dynamic Modeling and Control of Flexible Hexapod Platform for Micro-Vibration Isolation and Precision Tracking. *Appl. Mech. Mater.* **2014**, *490*, 412–420. [CrossRef]
9. Kong, Y.; Huang, H. Vibration isolation and dual-stage actuation pointing system for space precision payloads. *Acta Astronaut.* **2018**, *143*, 183–192. [CrossRef]
10. Yun, H.; Liu, L.; Li, Q.; Li, W.; Tang, L. Development of an isotropic Stewart platform for telescope secondary mirror. *Mech. Syst. Signal Process.* **2019**, *127*, 328–344. [CrossRef]
11. Jiao, J.; Wu, Y.; Yu, K.; Zhao, R. Dynamic modeling and experimental analyses of Stewart platform with flexible hinges. *J. Vib. Control* **2019**, *25*, 151–171. [CrossRef]
12. Zhao, Y.; Zhang, C.; Zhang, D.; Shi, Z.; Zhao, T. Mathematical model and calibration experiment of a large measurement range flexible joints 6-UPUR six-axis force sensor. *Sensors* **2016**, *16*, 1271. [CrossRef]
13. Yang, X.L.; Wu, H.T.; Chen, B.; Kang, S.Z.; Cheng, S. Dynamic modeling and decoupled control of a flexible Stewart platform for vibration isolation. *J. Sound Vib.* **2019**, *439*, 398–412. [CrossRef]
14. Wang, C.; Xie, X.; Chen, Y.; Zhang, Z. Investigation on active vibration isolation of a Stewart platform with piezoelectric actuators. *J. Sound Vib.* **2016**, *383*, 1–19. [CrossRef]
15. Merriam, E.G.; Lund, J.M.; Howell, L.L. Compound joints: Behavior and benefits of flexure arrays. *Precis. Eng.* **2016**, *45*, 79–89. [CrossRef]
16. Jing, Z.; Xu, Q.; Huang, J. A review on kinematic analysis and dynamic stable control of space flexible manipulators. *Aerosp. Syst.* **2019**, *2*, 1–14. [CrossRef]
17. Rossell, J.M.; Vicente-Rodrigo, J.; Rubió-Massegú, J.; Barcons Xixons, V. An Effective Strategy of Real-Time Vision-Based Control for a Stewart Platform. In Proceedings of the 2018 IEEE International Conference on Industrial Technology (ICIT), Lyon, France, 19–22 February 2018; pp. 75–80.
18. Min, D.; Huang, D.; Su, H. High-Precision Tracking of Cubic Stewart Platform Using Active Disturbance Rejection Control. In Proceedings of the 2019 Chinese Control Conference (CCC), Guangzhou, China, 27–30 July 2019; pp. 3102–3107.
19. Zheng, Y.; Li, Q.; Yan, B.; Luo, Y.; Zhang, X. A Stewart isolator with high-static-low-dynamic stiffness struts based on negative stiffness magnetic springs. *J. Sound Vib.* **2018**, *422*, 390–408. [CrossRef]
20. Majercsik, L. On the semiactive control of a Stewart platform with flexible joints. *Rom. J. Mech.* **2019**, *4*, 27–38.
21. Wen, S.; Jing, J.; Cui, D.; Wu, Z.; Liu, W.; Li, F. Vibration isolation of a double-layered Stewart platform with local oscillators. *Mech. Adv. Mater. Struct.* **2021**, *29*, 6685–6693. [CrossRef]
22. Li, K.; Pan, B.; Gao, W.; Feng, H.-b.; Fu, Y.-l.; Wang, S.-g. Miniature 6-axis force/torque sensor for force feedback in robot-assisted minimally invasive surgery. *J. Cent. South Univ.* **2015**, *22*, 4566–4577. [CrossRef]
23. Zhou, S.; Sun, J.; Chen, W.; Li, W.; Gao, F. Method of designing a six-axis force sensor for stiffness decoupling based on Stewart platform. *Measurement* **2019**, *148*, 106966. [CrossRef]
24. Shi, Z.P.; Ding, C.T.; Zhao, Y.Z.; Zhao, T.S. Error Factors Analysis of Large Range Flexible Jionts Six-Axis Force Sensor. *Appl. Mech. Mater.* **2012**, *130*, 4232–4235. [CrossRef]
25. Qin, C.; Xu, Z.; Xia, M.; He, S.; Zhang, J. Design and optimization of the micro-vibration isolation system for large space telescope. *J. Sound Vib.* **2020**, *482*, 115461. [CrossRef]
26. Yang, J.; Xu, Z.; Wu, Q.; Wang, Z.; Li, H.; He, S. Design of a vibration isolation system for the space telescope. *J. Guid. Control Dyn.* **2015**, *38*, 2441–2448. [CrossRef]
27. Preumont, A.; Horodinca, M.; Romanescu, I.; de Marneffe, B.; Avraam, M.; Deraemaeker, A. A six-axis single-stage active vibration isolator based on Stewart platform. *J. Sound Vib.* **2007**, *300*, 644–661. [CrossRef]
28. Templeman, J.O.; Sheil, B.B.; Sun, T. Multi-axis force sensors: A state-of-the-art review. *Sens. Actuators A Phys.* **2020**, *304*, 111772. [CrossRef]
29. Aggogeri, F.; Borboni, A.; Faglia, R.; Merlo, A.; de Cristofaro, S. Precision Positioning Systems: An overview of the state of art. *Appl. Mech. Mater.* **2013**, *336*, 1170–1173. [CrossRef]
30. Wang, S.C.; Hikita, H.; Kubo, H.; Zhao, Y.-S.; Huang, Z.; Ifukube, T. Kinematics and dynamics of a 6 degree-of-freedom fully parallel manipulator with elastic joints. *Mech. Mach. Theory* **2003**, *38*, 439–461. [CrossRef]
31. Yao, J.; Zu, L.; Ruan, H.; Cai, D.; Bai, H.; Xu, Y.; Zhao, Y. Stiffness modeling and force mapping analysis of hybrid-limb six-axis force sensor. *Proc. Inst. Mech. Eng. C J. Mech. Eng. Sci.* **2021**, *235*, 908–919. [CrossRef]
32. Furqan, M.; Suhaib, M.; Ahmad, N. Dynamic analysis of six-axis Stewart platform using flexible joints. *Int. J. Mech. Robot. Syst.* **2018**, *4*, 214–233. [CrossRef]
33. Du, Z.; Shi, R.; Dong, W. A piezo-actuated high-precision flexible parallel pointing mechanism: Conceptual design, development, and experiments. *IEEE Trans. Robot.* **2013**, *30*, 131–137. [CrossRef]

34. Ranganath, R.; Nair, P.S.; Mruthyunjaya, T.S.; Ghosal, A. A force–torque sensor based on a Stewart Platform in a near-singular configuration. *Mech. Mach. Theory* **2004**, *39*, 971–998. [CrossRef]
35. Mohammed, H.M.; Deji, H. Research on 6 dof-stewart platform mechanical characteristics analysis and optimization design. *Int. J. Sci. Res.* **2013**, *2*, 391–395.
36. Jiang, H.; He, J.; Tong, Z.; Wang, W. Dynamic isotropic design for modified Gough–Stewart platforms lying on a pair of circular hyperboloids. *Mech. Mach. Theory* **2011**, *46*, 1301–1315. [CrossRef]